Journal of Fluids and Structures (1999) **13,** 103–126
Article No.: jfls1998.0185
All articles available online at http://www.idealibrary.com on IDEAL

A THEORETICAL MODEL FOR NONLINEAR PLANAR MOTIONS OF ROTORS UNDER FLUID CONFINEMENT

J. Antunes, J. Mendes, M. Moreira

Instituto Técnológico e Nuclear, Applied Dynamics Laboratory, ITN/ADL
2686 Sacavém Codex, Portugal

AND

T. Grunenwald

Commissariat à l'Energie Atomique, Département de Mécanique et Technologie, CEA/DMT
91191 Gif-sur-Yvette Cedex, France

(Received 27 April 1998 and in revised form 7 September 1998)

Following previous papers by Axisa, Antunes and co-workers, the authors address a theoretical model for immersed rotors, under moderate confinement, using simplified flow equations on the gap-averaged fluctuating quantities. However, in contrast to our previous efforts, the nonlinear terms of the flow equations are here fully accounted. Because such nonlinear analysis is quite involved, this paper will focus on the simpler case of planar motions, in order to emphasize the main aspects of our approach. A direct integration of the continuity and momentum equations leads to extremely lengthy formulations. Here, in order to solve the flow equations, we perform an exact integration of the continuity equation and an approximate solution of the momentum equation, based on a Fourier representation of the azimuthal pressure gradient. Then, an exact formulation for the dynamic flow force can be obtained. Our solution is discussed in connection with physical phenomena. Numerical simulations of the nonlinear rotor-flow coupled system are presented, showing that the linearized and the fully nonlinear models produces similar results when the eccentricity and the spinning velocity are low. However, if such conditions are not met, the qualitative dynamics stemming from these models are quite distinct. Experimental results indicate that the nonlinear flow model leads to better predictions of the rotor dynamics when the eccentricity is significant, when approaching instability and for linearly unstable regimes.

1. INTRODUCTION

Vibration of rotating shafts subjected to fluid–structure interaction is a physical problem of both theoretical significance and practical importance. By far, the most dangerous problems arise when rotor velocities lead to unstable regimes, with possible catastrophic consequences [see, for example, books by Vance (1988), Goodwin (1989), Frêne *et al.* (1990), Lalanne & Ferraris (1990), Childs (1993) and Hamrock (1994)]. A large amount of research work has been performed for very small gap configurations, such as found in bearings and seals. Several aspects of research in this area may be found, for example, in papers by Badgeley & Booker (1969), Holmes (1970), Brindley *et al.* (1983), Childs (1983), Myers (1984), Nelson (1985), Muszinska (1988), Nordmann *et al.* (1989) and Baskharone & Hensel (1991).

0889–9746/99/010103 + 24 $30.00

Larger gap geometries—which are of interest in pump systems and several other industrial applications—are not so well decumented. For these conigurations, the reduced gap $\delta = H/R$ (where H is the average annular gap and R is the rotor radius) is typically 0·1—two orders of magnitude greater than in bearings (where $\delta \approx 0{\cdot}001$). As a consequence, vibrations in larger gap geometries are characterized by values of the Reynolds number which are much greater than in bearing configurations. Therefore, while the dominant forces in bearings stem from fluid viscosity, inertial fluid effects are of paramount importance in larger gap annulus, leading to a specific dynamic behaviour of such systems.

Work on rotor dynamics under moderate fluid confinement was pioneered by Black (1969), Fritz (1970) and Hirs (1973), who stated the basic simplifying assumptions to model the flow in the annular gap. Further relevant work was presented by Ramsden *et al.* (1974, 1975). In several previous papers (Grunenwald *et al.* 1991; Axisa & Antunes 1992; Grunenwald 1994; Antunes *et al.* 1996), the authors have developed a thorough analysis of these systems, under the assumption of centered or eccentric fluid annuli. In those papers, rotor dynamics were modelled using linearized flow equations on the gap-averaged fluctuating quantities. Such simplified models enabled us to predict with reasonable success the modal parameters of the coupled system and the stability boundaries, as a function of the annulus geometry and rotor spinning velocity Ω.

Experimental validation has been provided, with a reasonable agreement (Antunes *et al.* 1992, 1995; Grunenwald *et al.* 1996). However, our experiments have also shown a progressive deterioration of the theoretical predictions at high spinning velocities, as well as at large eccentricities (see Figure 1). In spite of some experimental inadequacies, it is reasonable to suspect that such deterioration might be due to nonlinear effects which became significant near and beyond the stability boundaries. Hence, better predictions might be produced if the nonlinear terms of the flow equations were fully accounted—an issue which is pursued in our recent work. Because such nonlinear analysis is quite involved, this paper will focus on the simpler case of planar motions, in order to emphasize the main aspects of the problem.

In our previous work, a perturbation analysis was used, in which the fluid forces were the result of a steady flow field (dependent on the rotor eccentricity ε) and a fluctuating flow field, which was computed using the linearized fluid equations. From such an approach, we obtained the coupling coefficients of the added mass matrix, a damping/gyroscopic matrix and a stiffness/circulatory matrix. Complex eigenvalue analysis enabled the computation of modal frequencies and damping ratios of the coupled system as a function of the rotor spinning velocity and other parameters. The stability of the rotor was also asserted—specifically, both static (divergence) or dynamic (flutter) instabilities were predicted, depending on the ranges of parameters Ω, δ and ε.

A solution of the fully nonlinear flow equations is more complex. Indeed, the direct integration of the continuity and momentum equations leads to extremely lengthy formulations, which are difficult to manipulate—even using symbolic computational tools. In this paper, we discuss a number of strategies to obtain approximate nonlinear solutions of the flow equations. We proceed with the actual approach used, which consists of the exact integration of the continuity equation and an approximate solution of the momentum equation, based on a Fourier representation of the azimuthal pressure gradient. We then obtain an exact formulation for the dynamic fluid force. Also, we present an analytical solution for squeeze-film dampers, which stems from the general formulation when $\Omega = 0$.

The solutions obtained are discussed in conjunction with physical phenomena. Numerical simulations of the nonlinear system dynamics are presented, which display some interesting features. In particular, the linearized and the fully nonlinear model produce very

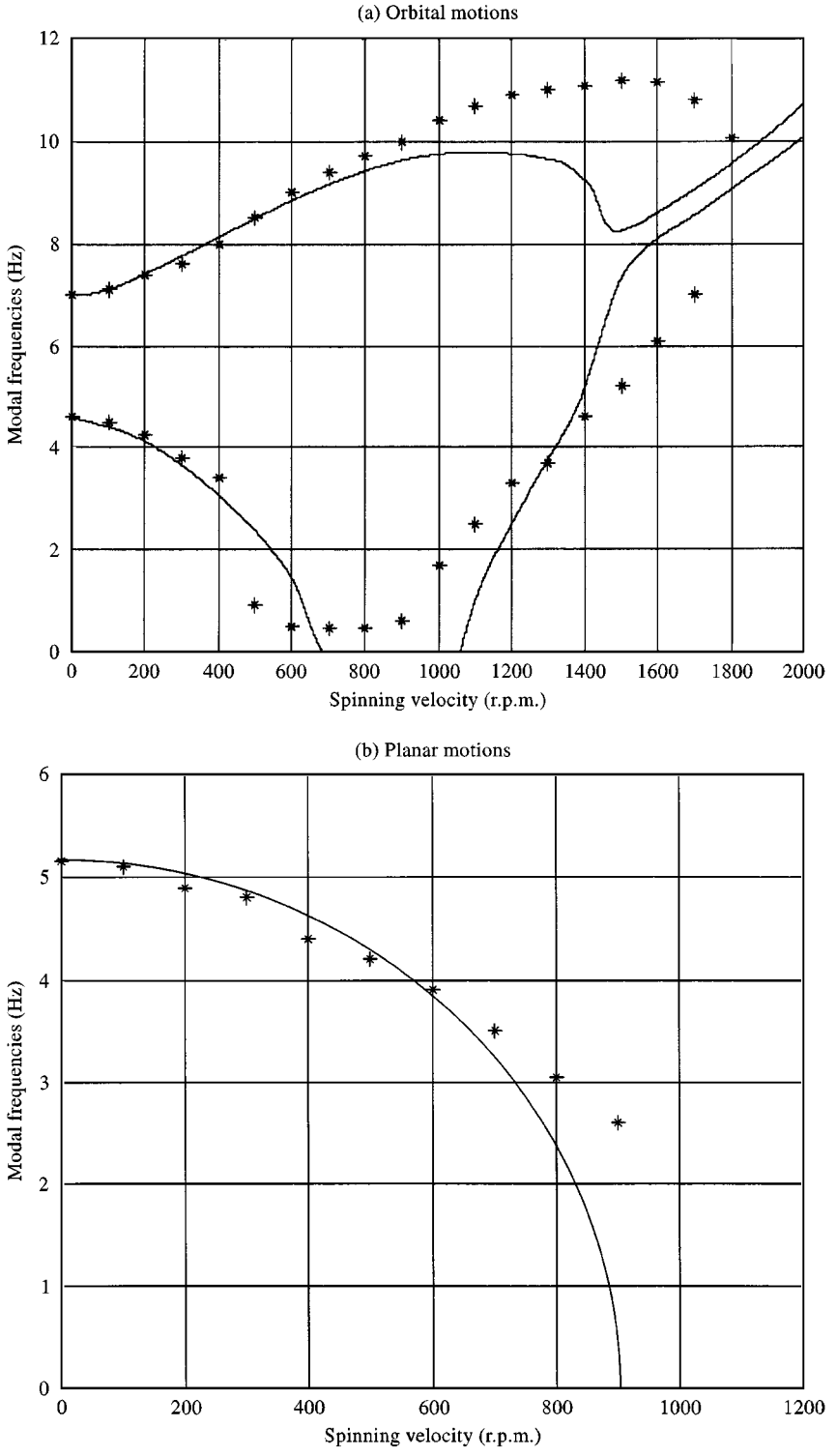

Figure 1. Modal frequencies as a function of the rotor spinning velocity (– , linear theory; *, experiments): (a) orbital motions: centred flow annulus using a rotor mounted on mildly asymmetric supports; (b) planar motions: eccentric flow annulus using a rotor mounted on very asymmetric supports.

similar results when the eccentricity and the spinning velocity are low. However, if such conditions are not met, the qualitative behaviour stemming from these models is quite distinct. Experimental results show that the nonlinear flow model leads to better predictions of the rotor dynamics when the eccentricity is significant, when approaching instability and also for linearly unstable regimes.

2. FLOW FORMULATION

The structure of co-rotating annular flows between coaxial nonvibrating cylinders is strongly dependent on the Reynolds number and the Taylor number of the flow, expressed as $\mathrm{Re} = 2HV/\nu$ and $\mathrm{Ta} = \mathrm{Re}\sqrt{H/R}$ (where V is an average flow velocity, dependent on the spinning velocity Ω of the inner cylinder)—see, for instance, Taylor (1936), Chandrasekhar (1961), Schlichting (1979), Tritton (1988), Sherman (1990) or Frêne (1990). For low values of Re and Ta, $\mathrm{Re} < 4000$ and $\mathrm{Ta} < 41$, when the inner cylinder rotates, the basic two-dimensional Couette flow is observed. When $\mathrm{Ta} > 41$, the flow displays structured three-dimensional Taylor vortices. If $\mathrm{Re} > 4000$, the flow becomes turbulent but still displays fairly organized vortices.

In order to deal with the vibratory problem, it is unreasonable to face a detailed model of such complex flow structures. Therefore, the following simplifying assumptions will be adopted, concerning the flow field: (i) the flow is modelled as being two-dimensional and incompressible, neglecting the radial graidents in the velocity and pressure fields; and (ii) the dissipative effects due to turbulent shear stresses at the walls are modelled using semi-empirical loss-of-head terms.

These assumptions are common when dealing with confined plane or annular flows, where the field properties may be conveniently averaged across the fluid depth [see Black (1969), Fritz (1970), Hirs (1973), Childs (1983), Nelson (1985), Axisa & Antunes (1992) or Antunes *et al.* (1996)].

Concerning the shear stresses, several empirical correlations relate the friction coefficient with the Reynolds number of the flow and other system parameters [see Wendt (1933), Vohr (1968), Yamada (1962), Constantinescu *et al.* (1975) and Hashimoto & Wada (1989)]. In the following analysis, as a final assumption, constant azimuthally averaged friction coefficients will be used, which are also assumed independent of the vibratory motion (Grunenwald 1994). The basic assumptions of the present work were adopted in order to obtain a set of flow equations which might be approached analytically. All aspects of the turbulent flow which are deemed too complex to be modelled in a simple way were integrated in a single empirical parameter—the flow-friction coefficient—which can be obtained from basic experiments. Hence, the subtleties of the true three-dimensional flow (such as the actual velocity profiles corresponding to Taylor vortices) are ignored when using this bulk-flow approach.

Obviously, the price to pay for these simplifying assumptions is that the validity of the theoretical model will diminish as the reduced gap of the annular flow increases. On the other hand, a less restrictive approach would inevitably lead to numerical computations of the three-dimensional highly turbulent flow [see, for example, relevant work by Arakere & Nelson (1988), Hirsch (1991), Mateescu *et al.* (1994, 1995) and Gwynllyw *et al.* (1996)]. Even when such heavier computations are feasible, it is harder to get insight from a set of specific numerical results than from simplified analytical solutions.

In this work, we consider a generic planar motion $X(t)$ represented in Figure 2. A detailed formulation for the flow equations has been presented elsewhere (Antunes *et al.* 1996) and will not be repeated here. Under the previous assumptions, one obtains the continuity

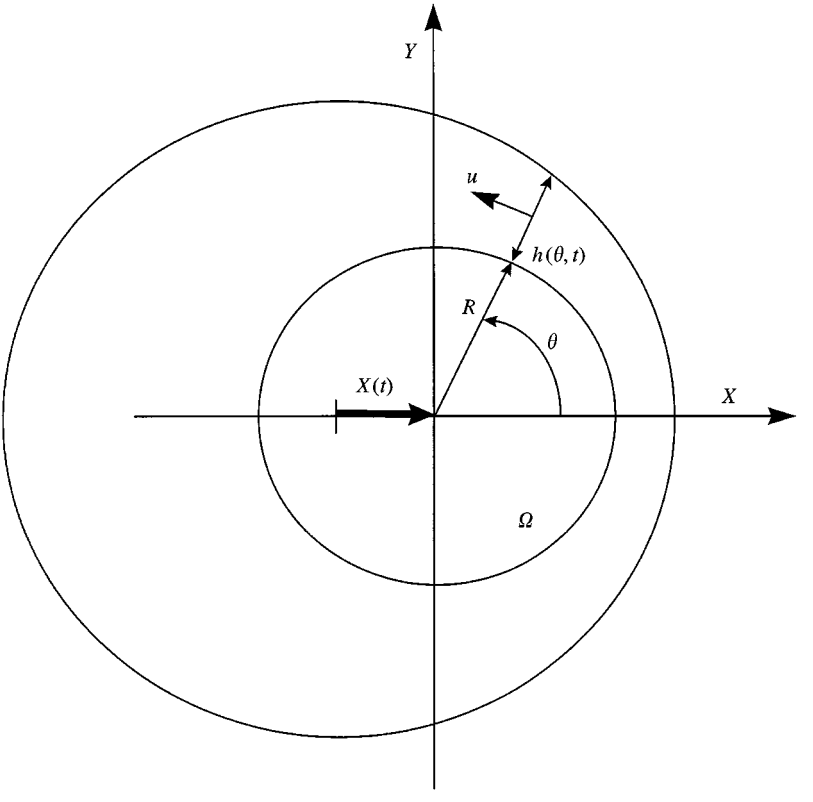

Figure 2. Geometry of the fluid annulus.

equation for incompressible flow,

$$\frac{\partial h}{\partial t} + \frac{1}{R}\frac{\partial}{\partial \theta}(hu) = 0, \tag{1}$$

where R is the shaft radius, $h(\theta, t)$ is the annular gap depth and $u(\theta, t)$ is the gap-averaged tangential flow velocity (see Figure 2). The momentum equation (projected in the tangential direction) is written as

$$\rho\left[\frac{\partial}{\partial t}(hu) + \frac{1}{R}\frac{\partial}{\partial \theta}(hu^2)\right] + \tau_s + \tau_r + \frac{h}{R}\frac{\partial p}{\partial \theta} = 0, \tag{2}$$

where ρ is the fluid density, p is the gap-averaged pressure and the shear stresses at the rotor and stator walls are given by

$$\tau_s = \tfrac{1}{2}\rho u|u| f_s,$$

$$\tau_r = -\tfrac{1}{2}\rho(\Omega R - u)|(\Omega R - u)| f_r, \tag{3}$$

where f_r and f_s are empirical friction coefficients, which depend on the flow Reynolds number and on wall roughness. Among several empirical correlations, those suggested by Wendt (1993) and Hirs (1973) are formulated as

$$f = a \times (\mathrm{Re})^b, \tag{4}$$

where coefficients a and b are obtained from experiments. A comprehensive analysis of friction correlations, in the context of the present work, was provided by Grunenwald (1994). The shear stresses change in a quadratic way with the flow velocity and always oppose the flow—hence the moduli in equations (3). This formulation may cause some analytical difficulties, which will be discussed later in the paper.

The planar motion $X(t)$, leads to a dynamic flow gap which is very well approximated by

$$h(\theta, t) \simeq H - X(t)\cos\theta. \tag{5}$$

We shall be interested in the resulting dynamic flow force,

$$F_X(t) = -LR\int_{-\pi}^{\pi} p(\theta, t)\cos\theta\,\mathrm{d}\theta, \tag{6}$$

where L is the immersed length of the rotor.

3. ANALYSIS OF THE FLOW EQUATION

3.1. Possible Approaches

Equations (1)–(3) are clearly nonlinear, and finding their analytical solution may be very difficult or even impossible. We begin by discussing several possible approaches to this problem and then present the actual method used in this work.

The direct solution of the flow equations seems quite straightforward and can be summarized as follows. From the continuity equation (1) with a dynamic gap (5), the fluctuating velocity $u(\theta, t)$ is computed by integration. Then, $u(\theta, t)$ is replaced in the momentum equation, and the pressure field $p(\theta, t)$ is computed by integrating equation (2) with equation (3). Pressure will depend on two unknown time-functions, $C(t)$ and $D(t)$, which stem from both integrations in θ. $C(t)$ is given implicitly by differential equation (26) by enforcing continuity on the pressure field over the annulus, which can be assumed when neglecting cavitation phenomena. We will not bother with $D(t)$ because this externally induced pressure term disappears when azimuthal integration (6) is finally applied to compute the resulting flow force. The problem with this simple approach is an exponential growth of the computations. After the integration of the momentum equation, one already obtains an extremely lengthy formulation for $p(\theta, t)$. This leads to a tedious estimation of $C(t)$ and renders the final integration (6) very problematic.

A different approach involves perturbation methods such as that of Lindstedt–Poincaré [see, for instance, Khalil (1996) or Verhulst (1996)]. The pressure and velocity fields are assumed in the form

$$p(\theta, t) \approx \sum_{m=0}^{M} \varepsilon^m p_m(\theta, t), \tag{7}$$

$$u(\theta, t) \approx \sum_{m=0}^{M} \varepsilon^m u_m(\theta, t). \tag{8}$$

When series (7) and (8) are replaced in equations (1) and (2), the original nonlinear problem leads to a sesquence of linear equations where each term $p_m(\theta, t)$ is obtained from the previous $p_{m-1}(\theta, t)$ terms. A solution is obtained if such series converge. Unfortunately, for the large rotor motions of interest here, many terms must be included in (7) and (8) to get an adequate approximation of the velocity and pressure fields. Therefore, this approach also leads to unmanageable computations.

For a circular geometry it is tempting to solve equations (1)–(3) using a Fourier series formulation for the pressure and velocity fields:

$$p(\theta, t) \approx A_0(t) + \sum_{n=1}^{N} [B_n(t)\sin(n\theta) + C_n(t)\cos(n\theta)], \tag{9}$$

$$u(\theta, t) \approx D_0(t) + \sum_{n=1}^{N} [E_n(t)\sin(n\theta) + F_n(t)\cos(n\theta)]. \tag{10}$$

When equations (9) and (10) are replaced in the continuity and momentum equations, one obtains a system of $2N$ ODEs in terms of the time-functions $A_0(t)$, $B_n(t)$, $C_n(t)$, $D_0(t)$, $E_n(t)$ and $F_n(t)$. Because these equations are nonlinearly coupled, their analytical solution is problematic and a time-step integration procedure must usually be used. A second drawback is that many terms must be accounted for in equations (9) and (10) to obtain an adequate representation of $u(\theta, t)$ and $p(\theta, t)$ for large rotor motions.

3.2. Adopted Approach

A mixed approach which proved fruitful was adopted in the present work, which is now summarized as follows. Because $u(\theta, t)$ can easily be obtained by integrating the continuity equation, a direct approach is followed at this stage. Hence, from equations (1) and (5), an exact formulation for the velocity field is obtained, which includes the unknown function $C(t)$:

$$u(\theta, t) = \mathbb{F}_1[X(t), \dot{X}(t), C(t), \theta]. \tag{11}$$

However, after replacing $h(\theta, t)$ and $u(\theta, t)$ in the momentum equation, which then reads

$$\frac{\partial p(\theta, t)}{\partial \theta} = \mathbb{F}_2[X(t), \dot{X}(t), \ddot{X}(t), C(t), \dot{C}(t), \theta], \tag{12}$$

the pressure gradient is assumed in Fourier series form:

$$\frac{\partial p(\theta, t)}{\partial \theta} \approx A_0(t) + \sum_{n=1}^{N} [B_n(t)\sin(n\theta) + C_n(t)\cos(n\theta)], \tag{13}$$

where

$$A_0(t) = \frac{1}{2\pi}\int_{-\pi}^{\pi} \mathbb{F}_2[X(t), \dot{X}(t), \ddot{X}(t), C(t), \dot{C}(t), \theta]\, \mathrm{d}\theta, \tag{14}$$

$$B_n(t) = \frac{1}{\pi}\int_{-\pi}^{\pi} \mathbb{F}_2[X(t), \dot{X}(t), \ddot{X}(t), C(t), \dot{C}(t), \theta]\sin(n\theta)\, \mathrm{d}\theta, \tag{15}$$

$$C_n(t) = \frac{1}{\pi}\int_{-\pi}^{\pi} \mathbb{F}_2[X(t), \dot{X}(t), \ddot{X}(t), C(t), \dot{C}(t), \theta]\cos(n\theta)\, \mathrm{d}\theta. \tag{16}$$

Then, from equations (13) the pressure field is easily obtained as

$$p(\theta, t) \approx A_0(t)\theta + \sum_{n=1}^{N} [-B_n(t)\cos(n\theta) + C_n(t)\sin(n\theta)], \tag{17}$$

where, to ensure the continuity of the pressure field, the following condition must apply:

$$A_0(t) = 0, \tag{18}$$

enabling the computation of $C(t)$.

For an adequate representation of this pressure field, a large number N of terms must still be included. However, we are mostly interested in the resultant fluid force $F_X(t)$ and not in $p(\theta, t)$. Hence, when formulation (17) is replaced in equation (6), the much simpler result is obtained

$$\begin{aligned} F_x(t) &= -LR\int_{-\pi}^{\pi}(-B_1(t)\cos^2\theta)\,\mathrm{d}\theta \\ &= \pi LRB_1(t), \end{aligned} \tag{19}$$

which stems from the orthogonality properties of $\sin(m\theta)$ and $\cos(n\theta)$. Therefore, only moderately difficult integrations leading to the terms $A_0(t)$ and $B_1(t)$ must be computed in order to obtain an exact solution for the nonlinear flow force $F_X(t)$

Before applying the previously described methodology to specific cases, one should notice that formulation (3) may cause some analytical difficulties, because the shear stresses are given in several branches according to the local value of the (gap-averaged) flow velocity $u(\theta, t)$:

$$\tau_s(\theta,t)+\tau_r(\theta,t)=\begin{cases} -\frac{1}{2}\rho u^2 f_s-\frac{1}{2}\rho(\Omega R-u)^2 f_r & \text{if } u/\Omega R\le 0,\\ \frac{1}{2}\rho u^2 f_s-\frac{1}{2}\rho(\Omega R-u)^2 f_r & \text{if } 0<u/\Omega R\le 1,\\ \frac{1}{2}\rho u^2 f_s+\frac{1}{2}\rho(\Omega R-u)^2 f_r & \text{if } u/\Omega R>1, \end{cases} \tag{20}$$

as shown in reduced form in Figure 3, for the specific case when $f_r = f_s = f$. Indeed, transitions between the branches of equation (20) cannot be decided *priori*, as they depend on the spinning velocity Ω and rotor vibratory motion $X(t)$, from which stems the velocity field $u(\theta, t)$. Such transitions are possible at low values Ω, when the vibratory motion may induce local flow velocities greater than ΩR or otherwise negative. Fortunately, this is rarely the case for the industrial components of practical concern, which rotate at significant spinning velocities or not at all. Namely, we can have one of the two situations discussed in the following.

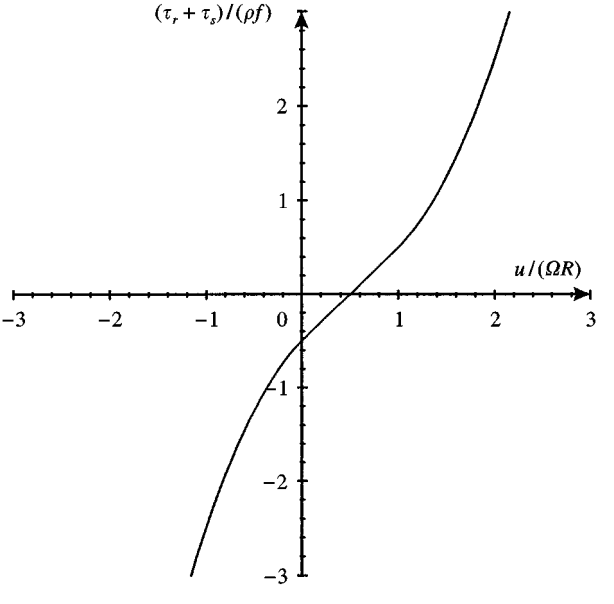

Figure 3. Skin-friction stresses as a function of the reduced flow velocity ($f_r = f_s = f$).

3.2.1. *Equipment with moderate-to-high spinning velocities* (*pumps, for instance*)

In this case, all dynamic conditions lead to flow velocities pertaining to the second branch of equation (20), and the shear stresses are given as

$$\tau_s(\theta, t) + \tau_r(\theta, t) = \frac{1}{2}\rho u^2 f_s - \frac{1}{2}\rho(\Omega R - u)^2 f_r \quad \text{with } 0 \le \frac{u}{\Omega R} \le 1. \tag{21}$$

3.2.2. *Equipment with zero spinning velocities* (*squeeze-film dampers*)

In this case, the flow velocity is positive (negative) along half of the shaft surface, while it is negative (positive) on the opposite side. Then, the first and third branches of (20) apply; thus,

$$\tau_s(\theta, t) + \tau_r(\theta, t) = \begin{cases} -\frac{1}{2}\rho u^2 f_s - \frac{1}{2}\rho u^2 f_r & \text{if } u \le 0, \\ \frac{1}{2}\rho u^2 f_s + \frac{1}{2}\rho u^2 f_r & \text{if } u > 0. \end{cases} \tag{22}$$

For planar motions, because of the symmetry of the problem, branching will unambiguously occur at $\theta = 0$ and $\theta = \pi$.

These two interesting cases will be now addressed, assuming that $f_r = f_s = f$. This convenient simplification is adequate, except in quite extreme conditions, such as when the roughness of the rotor and stator walls are very different (Grunenwald *et al.* 1996).

4. ANALYSIS OF ROTOR-FLOW SYSTEMS

4.1. Solution of the Flow Equations

From equation (1), the velocity field is obtained as

$$u(\theta, t) = \frac{R}{H - X(t)\cos\theta}(\dot{X}(t)\sin\theta + C(t)). \tag{23}$$

Then, from equations (2), (3) and (13), the pertinent time functions are obtained as

$$\begin{aligned} A_0(t) = &-2\rho R^2 H\dot{X}(t)C(t)G_3^{01}(t) + 2\rho R^2 X(t)\dot{X}(t)C(t)G_3^{00}(t) \\ &-\rho R^3\Omega f C(t)G_2^{00}(t) + \rho R^2(\tfrac{1}{2}R\Omega^2 f - \dot{C}(t))G_1^{00}(t), \end{aligned} \tag{24}$$

$$\begin{aligned} B_1(t) = &-\rho R^2 H(\dot{X}(t))^2 G_3^{11}(t) + \rho R^2 X(t)((\dot{X}(t))^2 + C^2(t))G_3^{10}(t) - \rho R^2(\dot{X}(t))^2 G_2^{11}(t) \\ &-\rho R^3\Omega f\dot{X}(t)G_2^{10}(t) - \rho R^2\ddot{X}(t)G_1^{10}(t), \end{aligned} \tag{25}$$

where each term $G_k^{ij}(t)$ is given by the first nonzero coefficient of the Fourier series of the function

$$F_k^{ij}(\theta, t) = \frac{(\sin\theta)^i(\cos\theta)^j}{[H - X(t)\cos\theta]^k}.$$

From equations (18) and (24), $C(t)$ is implicitly given by the differential equation

$$\dot{C}(t) + \frac{X(t)\dot{X}(t) + RH\Omega f}{H^2 - X^2(t)}C(t) = \frac{1}{2}R\Omega^2 f, \tag{26}$$

which unfortunately has not an explicit general solution. This aspect, which was already noticed before (Antunes *et al.* 1996), will be discussed in the following section. On the other

hand, equations (19) and (25) lead to the resultant flow force:

$$F_X(t) = -\pi\rho LR^3\left[2\frac{H-\sqrt{H^2-X^2(t)}}{X^2(t)}\ddot{X}(t)\right] - \pi\rho LR^3\left[2R\Omega f\frac{H-\sqrt{H^2-X^2(t)}}{X^2(t)\sqrt{H^2-X^2(t)}}\dot{X}(t)\right]$$
$$-\pi\rho LR^3\left[\frac{(H-\sqrt{H^2-X^2(t)})^2}{X^3(t)\sqrt{H^2-X^2(t)}}(\dot{X}(t))^2\right] - \pi\rho LR^3\left[-\frac{X(t)}{(H^2-X^2(t))^{3/2}}C(t)^2\right]. \tag{27}$$

4.2. Discussion of the Results

The stationary solution of equation (26) is formally given by

$$C(t) = \frac{1}{2}R\Omega^2 f\frac{\int[\exp\int F(t)\mathrm{d}t]\mathrm{d}t}{\exp\int F(t)\mathrm{d}t}, \tag{28}$$

where

$$F(t) = \frac{X(t)\dot{X}(t) + RH\Omega f}{H^2 - X^2(t)}. \tag{29}$$

Although a closed-form solution is not in general available, there are some specific cases where such a solution can be obtained.

4.2.1. *Linearized motions of a centred rotor*

For the linearized motions of a centred rotor, equation (26) reads

$$\dot{C}(t) + \frac{R\Omega f}{H}C(t) = \frac{1}{2}R\Omega^2 f, \tag{30}$$

leading to a constant stationary solution:

$$C(t) \equiv C_0 = \tfrac{1}{2}H\Omega. \tag{31}$$

The physical meaning of C_0 is highlighted when equation (31) is replaced in the linearized form of equation (23). Hence,

$$u(\theta, t) = \bar{U}_0 + \frac{R\Omega}{2H}X(t)\cos\theta + \frac{R}{H}\dot{X}(t)\sin\theta, \tag{32}$$

where the mean velocity of the bulk flow is given by

$$\bar{U}_0 = \frac{R}{H}C^0 = \frac{R\Omega}{2} \tag{33}$$

and we recover the classical assumption that the mean flow travels at half the tangential speed of the shaft wall (which is only strictly true for centred rotors with $f_r = f_s = f$). Under nonlinear conditions (large amplitude motions), the constant term (33) is replaced by a function $\bar{U}(t) = (R/H)C(t)$, which is the global bulk-flow velocity. From the linearized solution (27) and (31), the following force is obtained:

$$F_X(t) = -\frac{\pi\rho LR^3}{H}\left(\ddot{X}(t) + \frac{R\Omega f}{H}\dot{X}(t) - \frac{\Omega^2}{4}X(t)\right), \tag{34}$$

where one can recognize typical terms of added mass and flow damping, as well as a velocity-dependent negative flow-induced stiffness. Results (32)–(34) are in agreement with the previous linearized study by Axisa & Antunes (1992).

4.2.2. *Linearized motions of an eccentric rotor*

Let us consider now the linearized motions of an eccentric rotor, for a frictionless flow ($f = 0$). The rotor displacement $X(t)$ is given by a constant eccentricity X_0 and a (small) fluctuating term $X_1(t)$. Then, equation (26) leads to the following result:

$$C(t) = \frac{1}{2} H\Omega\left[1 - \left(\frac{X_0}{H}\right)^2\right] - \frac{1}{2}\frac{X_0}{H}\,\Omega X_1(t) \tag{35}$$

and, from the linearized form of equation (23), the velocity field follows

$$u(\theta, t) = \frac{R\Omega}{2H}\frac{H^2 - X_0^2}{H - X_0\cos\theta} + \frac{R\Omega}{2H}\left[\frac{(H^2 - X_0^2)\cos\theta}{(H - X_0\cos\theta)^2} - \frac{X_0}{H - X_0\cos\theta}\right]X_1(t)$$
$$+ R\,\frac{\sin\theta}{H - X_0\cos\theta}\,\dot{X}_1(t), \tag{36}$$

where one recognizes the eccentricity-dependent steady velocity of the co-rotating flow and the fluctuating terms. From equations (27) and (35) we obtain the corresponding fluctuating force:

$$F_X(t) = \frac{-\pi\rho \mathrm{L}\mathrm{R}^3}{\mathrm{H}}\left[-\frac{\Omega^2}{4}\frac{X_0\sqrt{H^2 - X_0^2}}{H}\right]\frac{-\pi\rho LR^3}{H}\left[\frac{2H^2 - 2H\sqrt{H^2 - X_0^2}}{X_0^2}\,\ddot{X}_1(t)\right]$$
$$\times\frac{-\pi\rho LR^3}{H}\left[-\frac{\Omega^2}{4}\frac{H}{\sqrt{H^2 - X_0^2}}\,X_1(t)\right], \tag{37}$$

which reproduces the previously obtained linearized results for eccentric configurations (Antunes *et al.* 1996). Furthermore, solutions (34) and (37) are identical for centred configurations with frictionless flow, as they should. The present nonlinear solution seems therefore quite plausible.

5. ANALYSIS OF THE SQUEEZE-FILM DAMPERS

5.1. Solution of the Flow Equations

In this case, the overall bulk-flow velocity is obviously null and it is easy to verify that the integration constant $C(t)$ must be null,

$$\int_{-\pi}^{\pi} u(\theta, t)\,\mathrm{d}\theta = 0 \Rightarrow C(t) = 0. \tag{38}$$

Thus from equation (23), the velocity field is given by

$$u(\theta, t) = \frac{R\dot{X}(t)\sin\theta}{H - X(t)\cos\theta}; \tag{39}$$

the flow field is anti-symmetric

$$u(\theta, t) = -u(-\theta, t), \tag{40}$$

and

$$\dot{X}(t) \geq 0 \Rightarrow \begin{cases} u(\theta, t) \geq 0 & \text{if } 0 \leq \theta \leq \pi, \\ u(\theta, t) \leq 0 & \text{if } -\pi \leq \theta \leq 0, \end{cases}$$
$$\dot{X}(t) \leq 0 \Rightarrow \begin{cases} u(\theta, t) \leq 0 & \text{if } 0 \leq \theta \leq \pi, \\ u(\theta, t) \geq 0 & \text{if } -\pi \leq \theta \leq 0. \end{cases} \tag{41}$$

Thus, equations (22) can be used without ambiguity. When computing $B_1(t)$, integration must proceed as follows:

$$B_1(t) = \frac{1}{\pi} \int_{-\pi}^{0} \mathbb{F}_2[X(t), \dot{X}(t), \ddot{X}(t), \theta] \sin\theta \, \mathrm{d}\theta + \frac{1}{\pi} \int_{0}^{\pi} \mathbb{F}_2[X(t), \dot{X}(t), \ddot{X}(t), \theta] \sin\theta \, \mathrm{d}\theta, \tag{42}$$

and one obtains the resultant fluid force

$$F_X(t) = -\pi\rho L R^3 \left[2 \frac{H - \sqrt{H^2 - X^2(t)}}{X^2(t)} \ddot{X}(t) \right] - \pi\rho L R^3 \left[\frac{(H - \sqrt{H^2 - X^2(t)})^2}{X^2(t)\sqrt{H^2 - X^2(t)}} (\dot{X}(t))^2 \right]$$
$$- \pi\rho L R^3 \left[\frac{2Rf}{\pi} \frac{2HX(t) + (H^2 - X^2(t)) \ln((H - X(t))/[H + X(t)])}{X^3(t)(H^2 - X^2(t))} \dot{X}(t)|\dot{X}(t)| \right]. \tag{43}$$

5.2. Discussion of the Results

The force in equation (43) has three terms: an unsteady inertia term, a convective inertia term and a dissipative term, respectively. When comparing our solution (43) with the long cylinder solution for the normal instantaneous squeeze film force in Lu & Rogers (1994), we observe that: (i) the unsteady inertia term is exactly the same in the two solutions; (ii) our convective inertia term is of the same order of magnitude as in Lu & Rogers' solution which is 8/5 greater; and (iii) our dissipative term is obviously qualitatively different, because it was deduced assuming a loss-of-head model while Lu & Rogers' model assumes viscous flow. However, for low Reynolds numbers and small instantaneous eccentricity, it can be shown that the two dissipative terms are of the same order of magnitude.

One can note that the first two terms of equation (43) are the same as in the nonlinear solution (27) of the rotor-flow problem. Obviously, the other terms of equation (27) do not appear in equation (43), because Ω and $C(t)$ are null. Notice that solution (27) is based on the assumption that the shear stresses were given by the second branch of equation (20). However, transitions between the different beanches are possible at low values of Ω, as mentioned before. This simplification leads to a nonlinear model (27) without a dissipative term dependent on $\dot{X}(t)|\dot{X}(t)|$ and independent of Ω. However, the squeeze-film solution (43) presents a new nonlinear term—which could "solve" the lack of such dissipative term in solution (27), when $\Omega = 0$:

$$F_B = -\pi\rho L R^3 \left[\frac{2Rf}{\pi} \frac{2HX(t) + (H^2 - X^2(t)) \ln([H - X(t)]/[H + X(t)])}{X^3(t)(H^2 - X^2(t))} \dot{X}(t)|\dot{X}(t)| \right].$$

Then, it is tempting to combine solution (27) and (42), in order to obtain an approximate general solution:

$$F_X(t) = -\pi\rho LR^3\left[2\frac{H-\sqrt{H^2-X^2(t)}}{X^2(t)}\ddot{X}(t)\right] - \pi\rho LR^3\left[2R\Omega f\frac{H-\sqrt{H^2-X^2(t)}}{X^2(t)\sqrt{H^2-X^2(t)}}\dot{X}(t)\right]$$
$$-\pi\rho LR^3\left[\frac{(H-\sqrt{H^2-X^2(t)})^2}{X^2(t)\sqrt{H^2-X^2(t)}}(\dot{X}(t))^2\right] - \pi\rho LR^3\left[-\frac{X(t)}{(H^2-X^2(t))^{3/2}}C^2(t)\right]$$
$$-\pi\rho LR^3\left[+\frac{2Rf}{\pi}\frac{2HX(t)+(H^2-X^2(t))\ln([H-X(t)]/[H+X(t)])}{X^3(t)(H^2-X^2(t))}\dot{X}(t)|\dot{X}(t)|\right]. \tag{44}$$

Indeed, note that formulation (44) leads to solution (43) when $\Omega = 0$. Also, the ratio between the second and the last term in (44)—the F_A and F_B dissipative terms,
BMP

$$\left|\frac{F_A}{F_B}\right| = \pi\frac{H\sqrt{H^2-X^2(t)}-(H^2-X^2(t))}{2HX(t)-(H^2-X^2(t))\ln([H-X(t)]/[H+X(t)])}\frac{\Omega X(t)}{|\dot{X}(t)|} \tag{45}$$

shows that the relative magnitude of the squeeze-film term decreases as the rotor spins faster. On the other hand, squeeze-film effects are comparatively higher when $X(t) \to H$, as expected.

6. ANALYSIS OF THE COUPLED SYSTEM

6.1. Rotor-Flow Dynamical Equations

The motion equation of the rotor-flow coupled system reads

$$M_2\ddot{X}(t) + C_s\dot{X}(t) + K_sX(t) = F_X(t) + F_e(t), \tag{46}$$

where $F_e(t)$ stands for any external forcing function, and $F_X(t)$ is given by the nonlinear fluidelastic force (27), together with equation (26) for $C(t)$. Under linearized conditions, equation (27) is replaced by formulation (34) or (37) and the autonomous version of equation (46) becomes

$$M_s\ddot{X}(t) + C_s\dot{X}(t) + K_sX(t) = F_X[X(t), \dot{X}(t), \ddot{X}(t)]$$
$$= M_f\ddot{X}(t) + C_f\dot{X}(t) + K_fX(t) \tag{47}$$

or

$$M_c\ddot{X}(t) + C_c\dot{X}(t) + K_cX(t) = 0, \tag{48}$$

where M_c, C_c and K_c are the coupling flow-structure operators. The modal frequencies and damping values, as well as the stability of the system, stem from the complex eigenvalues:

$$\lambda_j = \sigma_j + i\omega_j = \frac{-C_c \pm \sqrt{C_c^2 + 4M_cK_c}}{2M_c}. \tag{49}$$

For planar motions of immersed rotors, the modal frequency $\omega_j(\Omega)$ decreases when the spinning velocity is augmented, as shown in Figure 1(b). The corresponds to the first, lower branch of the modal chart of an orbiting rotor, as typically shown in Figure 1(a). For planar motions, the system becomes linearly unstable by divergence when the modal frequency

becomes null. Physically this is due to the negative flow-induced stiffness term in equations (34) or (37).

6.2. Simulation of the Nonlinear Motions

Under nonlinear conditions, the system responses must be computed by time-step integration of equation (46)—with the flow force (27) and some external excitation (for instance, to simulate the flow turbulence or a shaker). The implicit formulation for $C(t)$ is then easy to deal with, as equation (26) can be numerically integrated along with equation (46). It is convenient to formulate equations (26) and (46) as a system of three first-order coupled differential equations,

$$\begin{Bmatrix} \dot{\mathbb{Z}}_1 \\ \dot{\mathbb{Z}}_2 \\ \dot{\mathbb{Z}}_3 \end{Bmatrix} = \begin{Bmatrix} \mathbb{Z}_2 \\ \dfrac{\mathbb{F}[\mathbb{Z}_1, \mathbb{Z}_2, \mathbb{Z}_3]}{M_s + M_f[\mathbb{Z}_1]} + \dfrac{1}{M_s + M_f[\mathbb{Z}_1]} F_e(t) \\ \mathbb{G}[\mathbb{Z}_1, \mathbb{Z}_2]\mathbb{Z}_3 + \mathbb{H} \end{Bmatrix}, \tag{50}$$

where

$$\mathbb{Z}_1 \equiv X(t); \quad \mathbb{Z}_2 \equiv \dot{X}(t); \quad \mathbb{Z}_3 \equiv C(s)$$

and $\mathbb{F}, \mathbb{G}, \mathbb{M}_f$ are obvious, from equations (26) and (27).

Under linear conditions, when an explicit solution $C(t)$ is obtained, equation (50) leads simply to

$$\begin{Bmatrix} \dot{\mathbb{Z}}_1 \\ \dot{\mathbb{Z}}_2 \end{Bmatrix} = \begin{bmatrix} 0 & 1 \\ -\dfrac{K_c}{M_c} & -\dfrac{C_c}{M_c} \end{bmatrix} \begin{Bmatrix} \mathbb{Z}_1 \\ \mathbb{Z}_2 \end{Bmatrix} + \begin{Bmatrix} 0 \\ \dfrac{1}{M_c} F_e(t) \end{Bmatrix}. \tag{51}$$

Equation (50) was solved using an explicit algorithm of the Runge–Kutta type, with an error controlled time-step based on the fourth- and fifth-order approximations (Press *et al.* 1992; Shampine 1994). The external excitation was a Gaussian noise, low-pass filtered outside the frequency range $0 \sim 15$ Hz. The integration time-step was $\Delta t = 10^{-3}$ s, and 10 s of the system responses were simulated, for each spinning velocity. Numerical simulations were based on two configurations, as shown in Table 1.

Table 1

Parameters of the numerical simulations

	Rotor A	Rotor B
R (m)	0·044	0·047
H (m)	0·006	0·003
H/R	0·14	0·06
M_s (kg)	8	8
C_s (N s/m)	3	4
K_s (N/m)	$2{\cdot}2 \times 10^4$	$2{\cdot}2 \times 10^4$
M_f (kg)	14	43
C_v (N s/m)	53	189
ω_s (Hz)	8·3	8·3
ω_f (Hz)	5·0	3·3

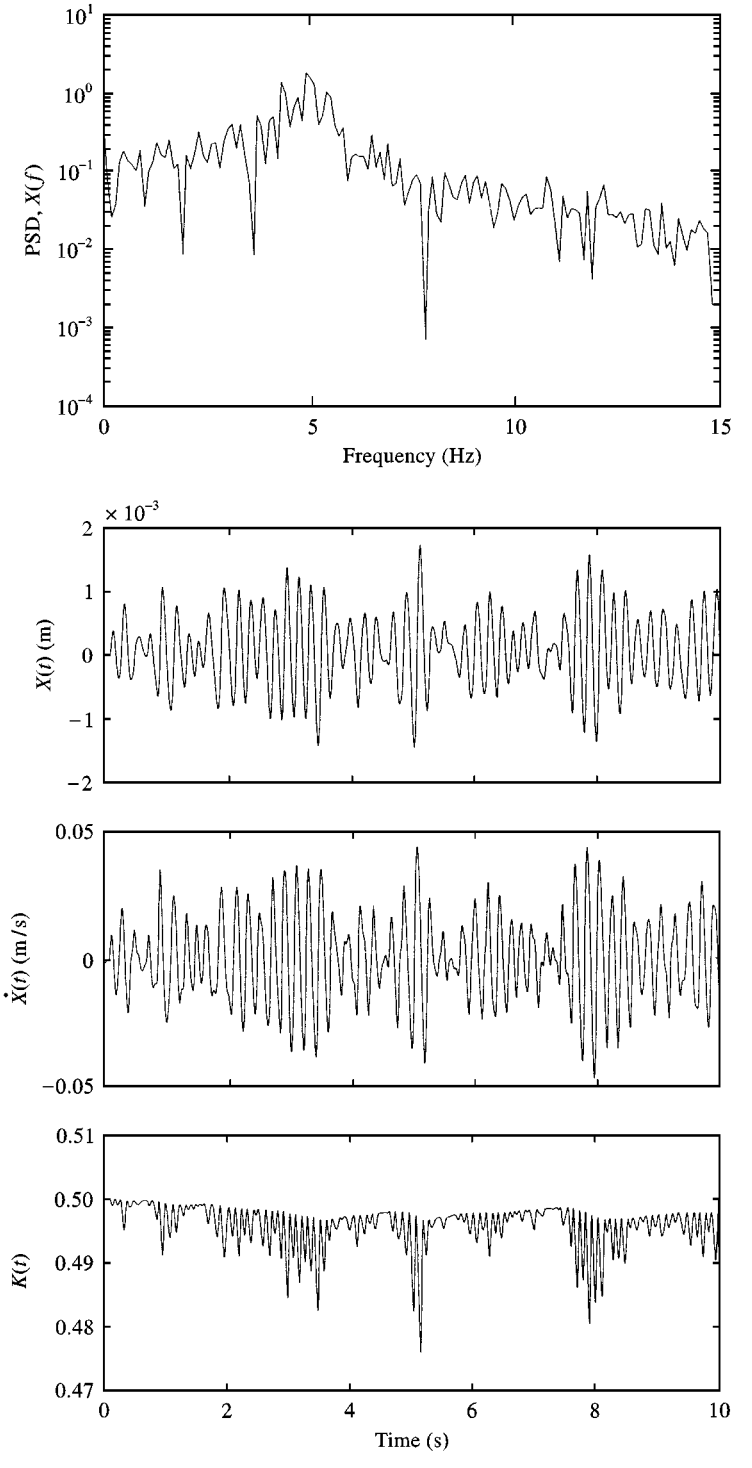

Figure 4. Vibratory response of *centred configuration* A at low spinning velocity (100 rpm).

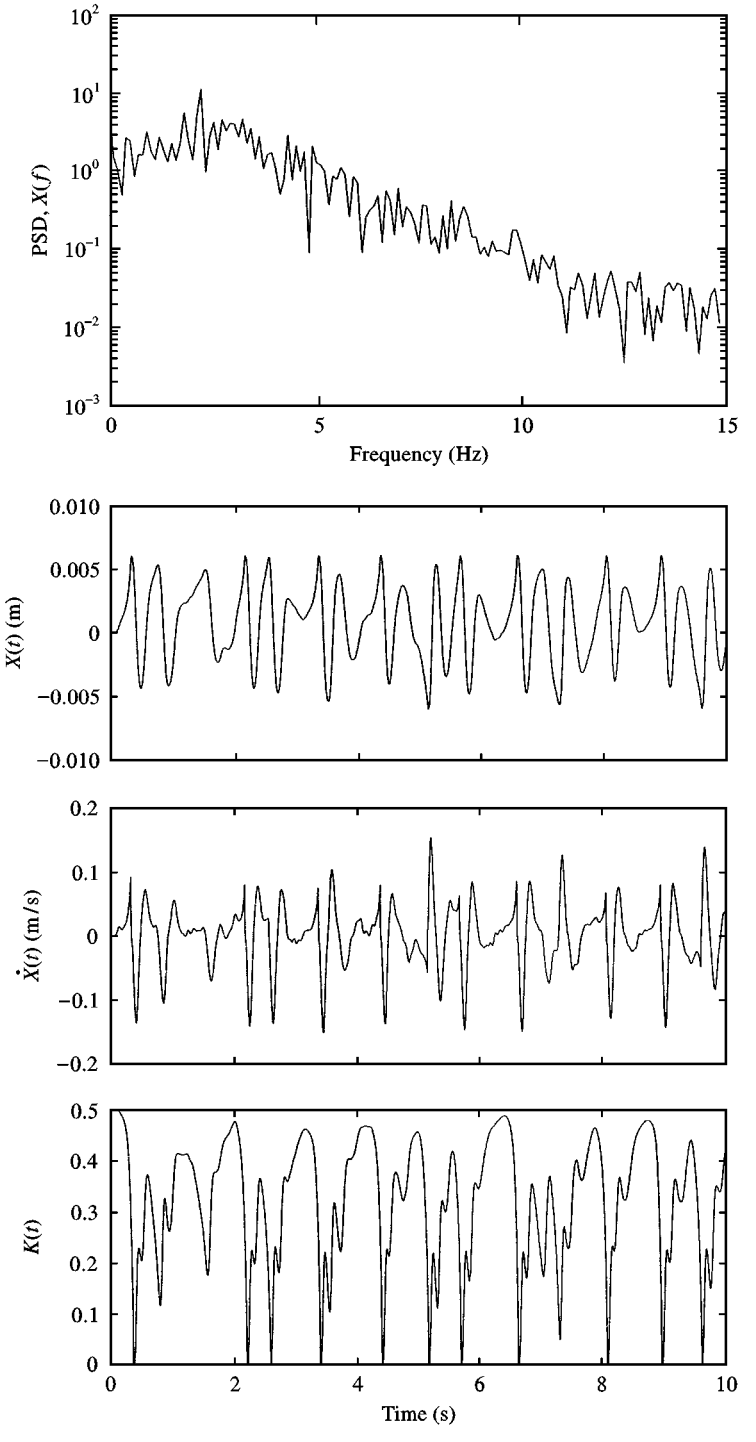

Figure 5. Vibratory response of *centred configuration* A at high spinning velocity (800 rpm).

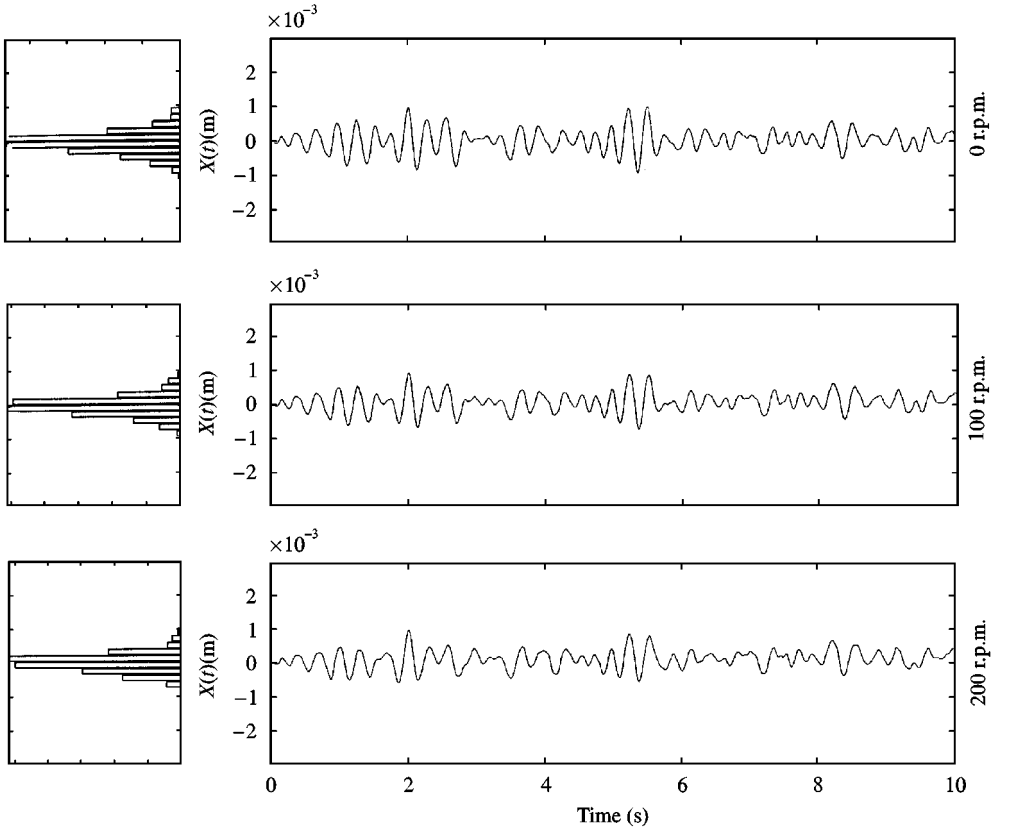

Figure 6. Vibratory response of *centred configuration* B as a function of the spinning velocity (0–200 rpm).

The modal frequencies of these configurations are compatible with the random excitation used. Furthermore, the parameters in Table 1 are those of our experimental set-up (Section 7.1). Here ω_s is the modal frequency of the structure in air and ω_f is the modal frequency of the nonrotating immersed rotor. The lower values of ω_f reflect the effect of the fluid added mass M_f—see equations (34) and (37). C_v is the viscous damping in still fluid, which is included with the structural damping C_s. A typical flow friction coefficient of $f = 0{\cdot}01$ was used when computing the dissipative terms related to the rotor velocity Ω. With both configurations, simulations were run for centered rotors and also for systems initially eccentric by 60% of the radial gap.

Figure 4 shows sample results obtained at a low spinning velocity (100 rpm), for *centred configuration* A. As expected, the response is almost Gaussian with maximum energy about 5 Hz, in agreement with Table 1. This can be observed in the spectrum of the response, as well as in the time-histories of the displacement and velocity. In the third time plot, the dimensionless function $K(t) = C(t)/(H\Omega)$ clearly approaches the theoretical value $\frac{1}{2}$ of the linearized analysis presented in Section 6.1. Hence, for low ecentricities and spinning velocities, the nonlinear flow formulation [equation (27) subject to equation (26)] leads to results which are almost identical to those stemming from our previous linearized analysis [equations (34) with (31)].

Figure 5 shows a completely different scenario. Indeed, the same configuration is now simulated at 800 rpm—a spinning velocity which is beyond the divergence instability

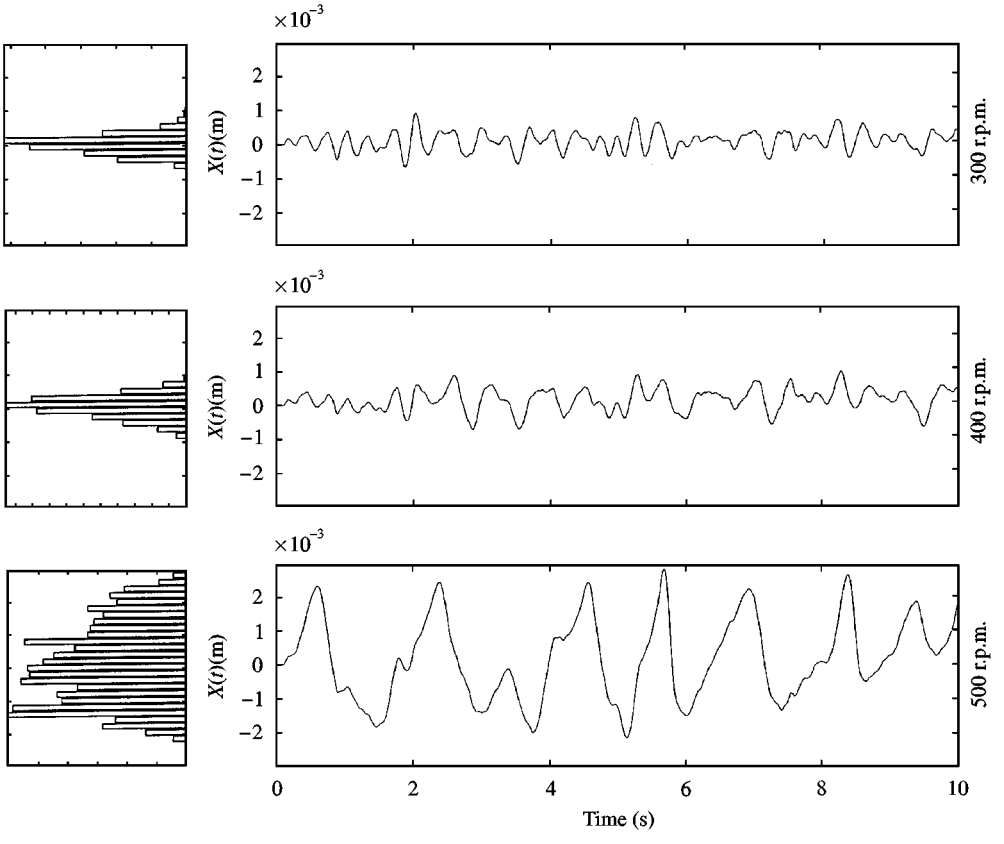

Figure 7. Vibratory response of *centred configuration* B as a function of the spinning velocity (300–500 rpm).

threshold (at about 750 rpm). Here the rotor vibration is very nonlinear and motion amplitudes are enough to overcome the annular gap. The obstruction of the co-rotating flow is displayed by the sudden decreases in $\bar{U}(t)$.

Obviously, a linearized solution is now far from the actual nonlinear dynamics of the system. A systematic picture of the typical rotor dynamics is presented in Figures 6–8. Here, time-responses $X(t)$ of *centred configuration* B are shown as a function of Ω, together with the corresponding histograms. One can notice the progressive transition from Gaussian to non-Gaussian behaviour. Also the decrease of the response frequency, as predicted by linear theory, is followed by a progressive increase when nonlinear effects dominant (at about 500 rpm). The transition between 600 and 700 rpm is also interesting, because the essentially symmetrical motion is replaced by a very asymmetrical response. Such a behaviour is due to a significant Bernoulli effect in the flow, at higher spinning velocities, which induces an increase of rotor drift—see the first term of solution (37), as well as Antunes *et al.* (1996) and Grunenwald *et al.* (1996).

7. TEST RESULTS

7.1. Experimental Set-up

Tests were performed with the same setup used in previous work by Grunenwald *et al.* (1996), where experimental details are available. It consists of a vertical shaft with radius

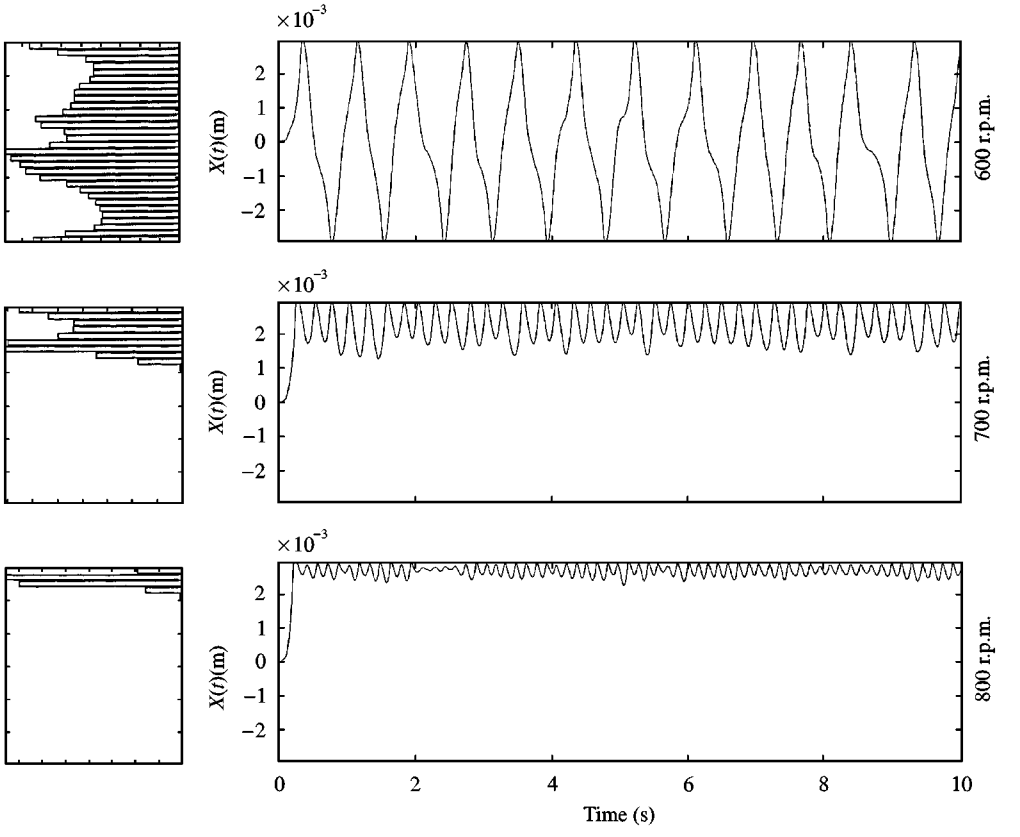

Figure 8. Vibratory response of *centred configuration* B as a function of the spinning velocity (600–800 rpm).

R (dependent on the configuration tested, see Table 1) and length $L = 250$ mm. The shaft is mounted using a pair of conical bearnings, assembled in a rigid support plate maintained by four flexible struts. Planar motions were insured by using asymmetric supports (with rectangular cross-section) providing $K_Y \gg K_X$. The shaft rotates inside a rigid outer shell, the full length of the annular gap being filled with water. The shaft-to-shell reduced eccentricity could be varied. Steady shaft rotation was provided by an electric motor, with precise velocity control, using a double Cardan joint for torque transmission. To avoid surface effects and flow ventilation at higher spinning velocities, a large-gap labyrinth was used which proved to be adequate. Rotor vibrations were sensed with an eddy-current displacement transducer, located near the support plate. Excitation was provided by a noncontacting electro-mechanical shaker, driven with filtered random noise. The excitation force was measured using a piezo-electric transducer. For several values of ε and Ω, the modal parameters of the coupled system and the nonlinear response frequencies were identified using our computer-based signal-processing software.

7.2. Rotor Dynamics

Figure 9 presents the theoretical and experimental response frequencies, as a function of Ω, for both *centred* and *eccentric configurations* B. Here the nonlinear numerical simulation

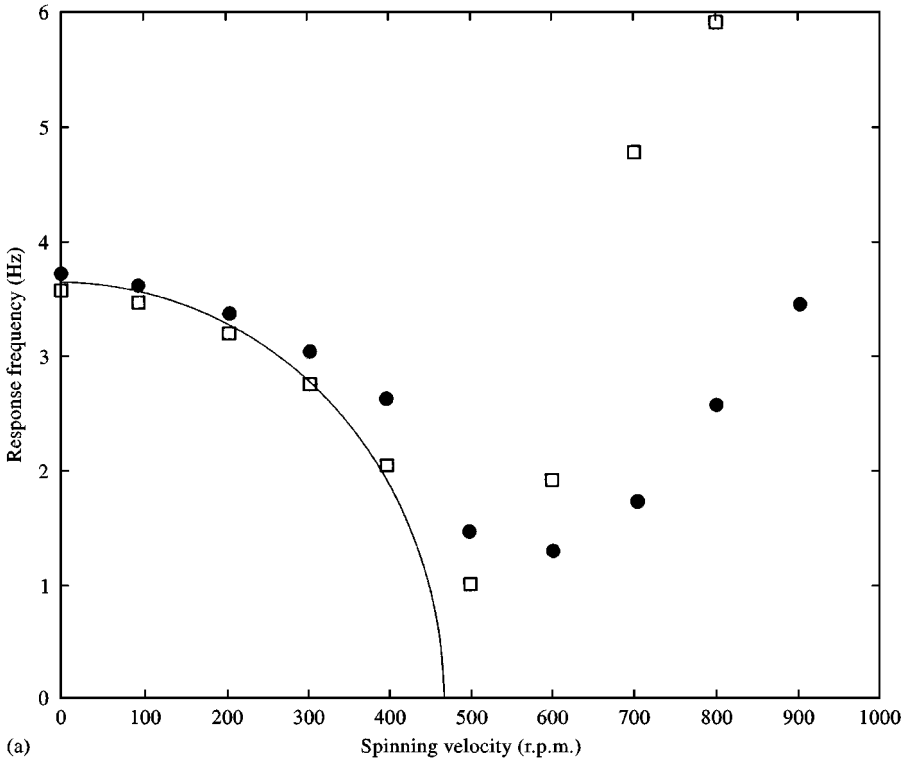

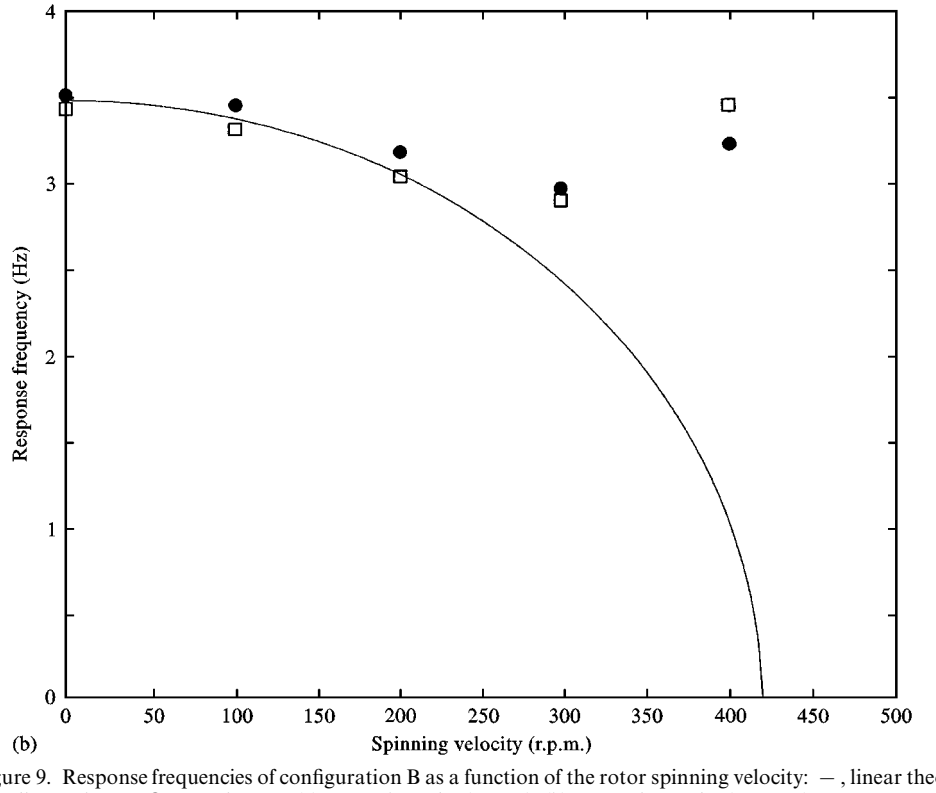

Figure 9. Response frequencies of configuration B as a function of the rotor spinning velocity: —, linear theory; □, nonlinear theory; ●, experiments, (a) centred results ($\varepsilon_0 = 0$); (b) eccentric results ($\varepsilon_0 = 0{\cdot}6$).

results are shown with the modal predictions issued from the linearized model. In both configurations, the nonlinear theory is in better agreement with the experimental results. For the centred case, departure from the linearized model arises only near the instability boundary. However, the nonlinear behaviour of the eccentric configuration is already displayed at lower spinning velocities. Some quantitative discrepancies between the theoretical and experimental results may be due to the three-dimensional axial structure of the flow, which was induced by a low value of the experimental ratio L/R. Such an effect is obviously not accounted for in the theoretical model [see also Grunenwald *et al.* (1996)].

8. CONCLUSIONS

In this paper, we presented a theoretical formulation for the nonlinear planar motions of a rotor immersed in a confined fluid. The solution approach in this work enabled us to keep analytical complexities at a manageable level. The nonlinear solution obtained is compatible with the linearised solutions previously developed by the authors. It provides insight on the system responses at higher eccentricities and spinning velocities. The qualitative agreement between the nonlinear theory and experimental results is encouraging, in spite of some quantitative discrepancies which might be due to the finite length of the experimental rotor. This nonlinear theoretical model is currently being extended to cope with three-dimensional orbital rotor motions.

ACKNOWLEDGEMENTS

The experimental work presented in this paper was achieved with the valuable contribution of Paulo de Araújo from ITN/Applied Dynamics Laboratory. Interesting discussions with C. Debailleux, from Lille University are acknowledged.

References

Antunes, J., Axisa, F. & Hareux, F. 1992 Flexural vibrations of rotors immersed in dense fluids: Part 2—experiments. *Journal of Fluids and Structures* **6,** 23–38.

Antunes, J., Grunenwald, T., Axisa, F. & Bennett, G. 1995 Vibrations and stability of asymmetrically supported rotors with annular fluid confinement. *International Conference on Structural Dynamics, Vibration, Noise and Control, SDVNC' 95*. Hong Kong, December 1995.

Antunes, J., Axisa, F. & Grunenwald, T. 1996 Dynamics of rotors immersed in eccentric annular flow: Part 1—theory. *Journal of Fluids and Structures* **10,** 893–918.

Arakere, N. & Nelson, H. 1988 An interior collocation method for static and dynamic analysis of finite length gas journal bearings. *ASME Journal of Tribology* **110,** 456–461.

Axisa, F. & Antunes, J. 1992 Flexural vibrations of rotors immersed in dense fluids: Part 1–theory. *Journal of Fluids and Structure* **6,** 3–21.

Badgeley, R. & Booker, J. 1969 Turborotor instability: Effect of initial transients on plane motion. *ASME Journal of Lubrication Technology* **91,** 625–633.

Baskharone, E. & Hensel, S. 1991 Moment coefficients of incompressible flow seals with conically whirling rotors. *International Journal of Mechanical Sciences* **33,** 151–167.

Black, H. 1969 Effects of hydraulic forces in annular pressure seals on the vibrations of centrifugal pump rotors. *I. Mech. E. Journal of Mechanical Engineering Science* **11,** 206–213.

Brindley, J., Elliot, L. & Mckay, J. 1983 The role of cavitation in whirl instability in a rotor bearing. *Journal of Applied Mechanics* **50,** 87–890.

Chandrasekhar, S. 1961 *Hydrodynamic and Hydromagnetic Stability*. New York: Dover.

Childs, D. 1983 Finite length solutions for rotordynamic coefficients of turbulent annular seals. *ASME Journal of Lubrication Technology* **105,** 437–444.

CHILDS, D. 1993 *Turbomachinery Rotordynamics*: *Phenomena, Modeling and Analysis*. New York: John Wiley & Sons.

CONSTANTINESCU, V., GALETUSE, S. & KENNEDY, F. 1975 On the comparison between lubrication theory, including turbulence and inertia forces and some existing experimental data. *ASME Journal of Lubrication Theory* **97,** 439–449.

FRÊNE, J. NICOLAS, D., DEGUEURCE, B. BERTHE, D. & GODET, M. 1990 *Lubrification Hydrodynamique*. Paris: Eyrolles.

FRITZ, R. 1970 The effects of an annular fluid on the vibrations of a long rotor: Part I—theory. *ASME Journal of Basic Engineering* **92,** 923–929.

GOODWIN, M. J. 1989 *Dynamics of Rotor-Bearing Systems*. London: Unwin Hyman.

GRUNENWALD, T., AXISA, F. & ANTUNES, J. 1991 Rotor vibration under fluid confinement: analysis of dissipative phenomena and stability. *Eighth World Congress on the Theory of Machines and Mechanisms*. Prague, August 1991.

GRUNENWALD, T. 1994 Comportement vibratoire d'arbres de Machines Tournantes dans un Espace Annulaire de Fluide de Confinement Modéré. Doctoral Thesis, Paris University, September 1994.

GRUNENWALD, T., AXISA, F., BENNETT, G. & ANTUNES, J. 1996 Dynamics of rotors immersed in eccentric annular flow: Part 2—experiments. *Journal of Fluids and Structures* **10,** 919–944.

GWYNLLYW, D., DAVIES, A. & PHILLIPS, T. 1996 A moving spectral element approach to the dynamically loaded journal bearing problem. *Journal of Computational Physics* **123,** 476–494.

HAMROCK, B. J. 1994 *Fundamentals of Fluid Film Lubrication*. New York: McGraw-Hill.

HASHIMOTO, H., WADA, S. 1989 Theoretical approach to turbulent lubrication problems including surface roughness effects. *ASME Journal of Tribology* **111,** 17–22.

HIRS, G. G. 1973 A bulk-flow theory for turbulence in lubricant films. *ASME Journal of Lubrication Technology* **95,** 137–146.

HIRSCH, C. 1991 *Numerical Computation of Internal and External Flows*. New York: John Wiley & Sons.

HOLMES, R. 1970 Non-linear performance of turbine bearings. *I. Mech. E. Journal of Mechanical Engineering Science* **12,** 337–380.

KHALIL, H. K. 1996 *Nonlinear Systems*. London: Prentice-Hall.

LALANNE, M. & FERRARIS, G. 1990 *Rotordynamics Predictions in Engineering*. New York: John Wiley & Sons.

LU, Y. and ROGERS, R. J. 1994 Normal instantaneous squeeze film force for a finite length cylinder. *ASME Journal of Tribology* **116,** 589–596.

MATEESCU, D., PAIDOUSSIS, M. & SIM, W. 1994 Spectral solutions for unsteady annular flows between eccentric cylinders induced by transverse oscillations. *Journal of Sound and Vibration* **117,** 635–649.

MATEESCU, D., PAIDOUSSIS, M. & SIM, W. 1995 Three-dimensional viscous flows between concentric cylinders executing axially variable oscillations: a hybrid spectral/finite difference solution. *Journal of Applied Mechanics* **62,** 667–673.

MYERS, C. 1984 Bifurcation theory applied to oil whirl in plain cylindrical journal bearings. *Journal of Applied Mechanics* **51,** 245–250.

MUSZINSKA, A. 1988 Stability of whirl and whip in rotor/bearing systems. *Journal of Sound and Vibration* **127,** 49–64.

NELSON, C. 1985 Rotordynamic coefficients for compressible flows in tapered annular seals. *ASME Journal of Tribology* **107,** 318–325.

NORDMANN, R., DIETZEN, F. & WEISER, H. 1989 Calculation of rotordynamic coefficients and leakage for annular gas seals by means of finite difference techniques. *ASME Journal of Tribology* **111,** 545–552.

PRESS, W., FLANNERY, B., TEUKOLSKY, S. & VETTERLING, W. 1992 *Numerical Recipes*: *The Art of Scientific Computing*. Cambridge: Cambridge University Press.

RAMSDEN, J., RITCHIE, G. & GUPTA, J. 1974 The vibrational response characteristics of a design for the sodium pumps of the commercial fast reactor. *Proceedings I.Mech.E. Fluid Machinery and Nuclear Energy Groups Convention*: *Pumps For Nuclear Power Plant*, Bath, April 1974. Paper C107/74, pp. 187–196.

RAMSDEN, J., JONES, H. & COWKING, E. 1975 Vibration of the P. F. R. primary sodium pumps. *Proceedings I. Mech. E. Conference on Vibrations and Noise in Pump, Fans and Compressor Installations*, Southampton, September 1975. Paper C103/75, pp. 21–33.

SCHLICHTING, H. 1979 *Boundary Layer Theory*. New York: McGraw-Hill.

SHAMPINE, L. F. 1994 *Numerical Solution of Ordinary Differential Equations*. New York: Chapman & Hall.
SHERMAN, F. S. 1990 *Viscous Flow*. New York: McGraw-Hill.
TAYLOR, G. I. 1936 Fluid friction between rotating cylinders. *Proceeding of the Royal Society A* **157,** 546–564.
TRITTON, D. J. 1988 *Physical Fluid Dynamics*. New York: Van Nostrand Reinhold.
VANCE, J. M. 1988 *Rotordynamics of Turbomachinery*. New York: John Wiley & Sons.
VERHULST, F. 1996 *Nonlinear Differential Equations and Dynamical Systems*. Berlin:Springer-Verlag.
VOHR, J. H. 1968 An experimental study of Taylor vortices and turbulence in flow between eccentric rotating cylinders. *ASME Journal of Lubrication Technology* **90,** 285–296.
WENDT, F. 1933 Turbulente Stomungen Zwischen Zwei Rotierenden Konaxialen Zylindern. *Ingenieur Archiv* **4,** 577–595.
YAMADA, Y. 1962 Resistance of flow through an annulus with an inner rotating cylinder. *Bulletin of the J.S.M.E.* **5,** 302–310.

APPENDIX: NOMENCLATURE

$A_n(t)$, $B_n(t)$, $C_n(t)$	Fourier coefficients of the pressure series formulation
$C(t)$	integration constant (related to the average bulk-flow velocity)
C_0	integration constant (stationary solution)
C_c	coefficient of velocity coupling in the flow–structure system
C_f	coefficient of velocity coupling by the flow
C_s	coefficient of structural damping
C_v	coefficient of viscosity damping
$h(\theta, t)$	local gap
f	friction coefficient
f_r	friction coefficient at the rotor wall
f_s	friction coefficient at the stator wall
F_X	coupling force by the flow
H	average annular gap
K	reduced average flow velocity
K_c	coefficient of displacement coupling in the flow–structure system
K_f	coefficient of displacement coupling by the flow
K_s	coefficient of structural stiffness
K_X	coefficient of structural stiffness (X-direction)
K_Y	coefficient of structural stiffness (Y-direction)
L	rotor length
M_c	coefficient of inertial coupling in the flow–structure system
M_f	coefficient of inertial coupling by the flow
M_s	coefficient of structural inertia
$p(\theta, t)$	local pressure
R	rotor radius
Re	Reynolds number of the flow
t	time
Ta	Taylor number of the flow
$u(\theta, t)$	local tangential velocity
$\bar{U}_0$	average bulk-flow velocity
$\bar{U}(t)$	global bulk-flow velocity
$X(t)$	rotor displacement
$\mathbb{Z}_1, \mathbb{Z}_2, \mathbb{Z}_3$	variables of the state-space formulation
δ	reduced gap
ε	rotor excentricity
λ_j	eigenvalues of the flow–structure system (mode j)
θ	azimuthal angle
ν	kinematic viscosity of the fluid
ρ	fluid density
σ_j	real part of the eigenvalues (related to damping)

τ_r	shear stresses at the rotor wall
τ_s	shear stresses at the stator wall
ω_j	circular frequency (mode j)
ω_s	modal frequency of the rotor (with no fluid)
ω_f	modal frequency of the flow–structure system
Ω	spinning velocity of the shaft